

Boson gas in a periodic array of tubes

P. Salas^{1,2}, F.J. Sevilla² and M.A. Solís²

¹*Posgrado en Ciencia e Ingeniería de Materiales, UNAM, Apdo. Postal 70-360, 04510 México, D.F., MEXICO*

²*Instituto de Física, UNAM, Apdo. Postal 20-364, 01000 México, D.F., MEXICO*
(ΩDated: November 10, 2018)

We report the thermodynamic properties of an ideal boson gas confined in an infinite periodic array of channels modeled by two, mutually perpendicular, Kronig-Penney delta-potentials. The particle's motion is hindered in the x - y directions, allowing tunneling of particles through the walls, while no confinement along the z direction is considered. It is shown that there exists a finite Bose-Einstein condensation (BEC) critical temperature T_c that decreases monotonically from the 3D ideal boson gas (IBG) value T_0 as the strength of confinement P_0 is increased while keeping the channel's cross section, $a_x a_y$ constant. In contrast, T_c is a non-monotonic function of the cross-section area for fixed P_0 . In addition to the BEC cusp, the specific heat exhibits a set of maxima and minima. The minimum located at the highest temperature is a clear signal of the confinement effect which occurs when the boson wavelength is twice the cross-section side size. This confinement is amplified when the wall strength is increased until a dimensional crossover from 3D to 1D is produced. Some of these features in the specific heat obtained from this simple model can be related, qualitatively, to at least two different experimental situations: ⁴He adsorbed within the interstitial channels of a bundle of carbon nanotubes and superconductor-multistrand-wires Nb₃Sn.

PACS numbers: 03.75.Hh; 05.30.Jp; 05.70.Ce; 67.40.Kh

I. INTRODUCTION

The properties of quantum systems at low dimensionality and temperature have attracted the attention of researchers for a long time. In particular, the study of phase transitions, such as superfluidity, superconductivity, or Bose-Einstein condensation, has been marked by an impressive interest among scientists in the field even though “true” long-range order phases are excluded by the Mermin-Wagner-Hohenberg theorem^{1,2} in dimensions lower or equal than two.

In two dimensions, however, the superfluid or superconductor transition arises by the acquisition of quasi-long-range-order in the system as described by the Kosterlitz-Thouless phase transition^{3,4}. This, has been experimentally confirmed in thin superconducting⁵⁻¹⁰ and helium-films¹¹⁻¹³. Historically, different experimental methods have been set up to study low dimensional phase transitions since the discovery of helium superfluidity. Indeed, studies on the behavior of helium films have been performed by using several experimental techniques, like the adsorption of helium on simple plane substrates¹⁴, or even on more complex ones as in nanoporous media such as cylindrical pores of Anopore¹⁵, Vycor¹⁶ or Gelsil¹⁷ glasses, where the effects of the substrate structure on the specific heat has been reported among other properties. More recently, studies of adsorption of atoms and molecules on planar substrates^{18,19}; the two-dimensional character of high critical temperature superconductivity; and the discovery of graphene, have made two-dimensional systems to be widely explored contrary to the case of quasi-one-dimensional ones.

Although the theoretical aspects of one-dimensional systems have been extensively studied²⁰, only very re-

cently 1D experimental reports have attracted a great attention. For example, now days it is possible to create a 1D Bose gas in cigar-shaped magneto-optic traps²¹ where the particle density, the cigar size and the intensity of the interaction between particles are experimentally tunable parameters, allowing one to examine quantum phenomena such as the superfluid to Mott-insulator phase transitions^{22,23}.

On the other hand, with the advent of carbon nanotubes, the realization of phase transitions in quasi-one-dimensional systems of different substances adsorbed on nanotube bundles is now possible²⁴⁻²⁷. The quasi-one-dimensional character of these structures is a consequence of the enormous aspect ratios that nanotubes exhibit, with cross-sections in the nanoscale regime. On such length scales the single-particle energy levels corresponding to the cross-section degrees of freedom are “frozen” leading to effective one-dimensional systems.

In some other recent theoretical studies^{28,29}, the occurrence of BEC of a weakly-interacting quantum gas of Bose particles (parahydrogen or ⁴He) adsorbed within the interstitial channels (IC) of a bundle of poly-disperse carbon nanotubes has been predicted. The reported BEC transition and particularly, the dependence of the specific heat on temperature, exhibit features of four dimensions in contrast to the expected one-dimensional behavior that has been, indeed, observed in the experimental report of Lasjaunias *et al.*³⁰ of the specific heat of adsorbed ⁴He in nanotubes. The authors of the former references, Refs. [28,29], argue that the presence of *nonuniformity* in the nanotube cross-section gives rise to three additional degrees of freedom (the radii of the three tubes that form the IC), needed in their analysis to ensure the occurrence of the BEC transition which, as they claim³¹ based on the results reported in Ref. [32], doesn't exist in

a uniform bundle of identical one-dimensional nanotubes.

Truly, it is well known that there is no BEC of a non-interacting boson gas in an impenetrable one-dimensional box potential. Also, that there is no BEC whenever the spatial dimensions of at least one direction is finite, thus excluding the possibility of BEC in just one channel. Therefore, a collection of independent IC's can not develop a BEC unless a coupling mechanism, such as tunnel-effect, is present between adjacent channels. A possible mechanism that couple the different IC's is considered in Refs. [28,29], where the authors argue that such a coupling leads to an effective density of states from which a non-vanishing BEC critical temperature is obtained. This effective density of states can be described as an inhomogeneously broadened convolution of the density of the heterogeneous transverse states with the one-dimensional density of states of a free particle that moves along the nanotube axis.

Here we suggest that the packing defects due to the heterogeneity of the nanotube cross-section³² may lead to a tunnel-effect-like mechanism that couples the different interstitial channels in the bundle, thus making BEC possible. Indeed, it is well known that suitable confinement potentials can make the BEC long-range-order character to be stable against long-range-fluctuations. Such is the case of the ideal Bose gas in two dimensions trapped by harmonic potentials, which undoubtedly undergoes BEC. So, even in the case of a collection of nanotubes with uniform cross-section, one would expect a BEC transition at a finite critical temperature when tunneling between neighboring channels (modeled using penetrable potential barriers) is considered.

In addition to the theoretical interest, the model presented in this paper can be applied to estimate critical temperatures and thermodynamic properties of superconductor-multistrand-wires whose technological applications, that go from Nuclear Magnetic Resonances to magnets used in high-energy accelerators, impel their understanding. For example, several authors report experimental studies on the thermodynamic properties of multistrand Nb₃Sn (an A15 type of superconductor) wires, that exhibit a transition temperature around 18 K and can support fields up to 15 Tesla³³. Typical numbers of filaments range from 10² to 10⁴ Nb₃Sn superconductor wires with diameters varying from a few to tens μ m. On the other hand, Nb₃Sn multifilament wires come in different sizes, shapes and compositions, depending on the techniques used to create them. The most common are the Bronze Route, the Internal Sn diffusion process and the Powder Metallurgy (PM) methods, and they may have a core either of Cu, Sn, NbSn or NbCu alloys, while usually immersed in Cu, and the use of tantalum and/or titanium barriers to prevent the Sn pollution in Cu³⁴. Experimentalists report either total specific heat curves and/or curves that subtract the normal state specific heat, to avoid phonon and unpaired electron interference^{33,35,36}. The main feature in this curves is the transition around 18 K with a typical width of 5

K. However, in some cases a second peak appears around 9 K which the authors interpret as the transition of the remnants of unreacted Nb. Here, in light of our results we suggest an alternative interpretation to the meaning of these maxima.

In this paper we report the thermodynamic properties with emphasis in the BEC critical temperature and the specific heat, of an ideal Bose gas within an infinite periodic array of tubes. Our results are benchmarks for ongoing studies on the properties of real spatially confined systems such as: a) He atoms in interstitial carbon nanotube bundles, b) Cooper pairs in periodic tubes like multistrand Nb₃Sn bundles or Bechgaard-salts³⁷ or c) bosonic atoms in two dimensional opto-magnetic traps²².

Although at very low (or zero) temperatures and/or high densities the interaction between particles cannot be neglected, we focus on an interactionless boson gas to study the effects of a periodic confining potential on the properties of the system. We show that this simple model captures qualitatively the properties of real systems, including the emergence of thermal phase transitions and/or dimensional crossovers^{38,39}.

In the following section we describe our system model. In Sec. III we calculate the Bose-Einstein condensation critical temperature in addition to the specific heat and other relevant thermodynamic variables. In Sec. IV we discuss the results and present our conclusions.

II. PERIODIC TUBE BUNDLES

Our system model consists of N non-interacting bosons confined in an infinite periodical array of penetrable tubes of rectangular cross section of sides a_x and a_y , and infinite length. We model the tubes array by considering two perpendicular Kronig-Penney (KP) delta barriers in the x and y directions with no constraints in the remaining z direction (see Fig. 1). Our periodic structure resembles either the bundle of homogeneous nanotubes, the superconductor-multistrand-wires or the experimental 2D periodic lattice of tightly confined potential tubes created in Ref. [22]. If the interaction between bosons is ignored, the Schrödinger equation for each boson of mass m in this system is

$$\left\{ -\frac{\hbar^2}{2m}\nabla^2 + V(x, y) \right\} \psi(x, y, z) = \varepsilon_k \psi(x, y, z) \quad (1)$$

with

$$V(x, y) = \sum_{n=-\infty}^{\infty} v_x \delta(x - na_x) + \sum_{n=-\infty}^{\infty} v_y \delta(y - na_y) \quad (2)$$

where v_x and v_y are the delta strength in the x and y directions, respectively.

The Schrödinger equation (1) is separable in each direction such that $\varepsilon_k = \varepsilon_{k_x} + \varepsilon_{k_y} + \varepsilon_{k_z}$ is the energy per particle, where

$$\varepsilon_{k_z} = \frac{\hbar^2 k_z^2}{2m}, \quad (3)$$

with $k_z = 2\pi n_z/L$ the momentum in the z -direction, $n_z = 0, \pm 1, \pm 2, \dots$ due to the periodic boundary conditions in a box of length L , and $\varepsilon_{k_{x,y}}$ are implicitly obtained from the equations⁴⁰

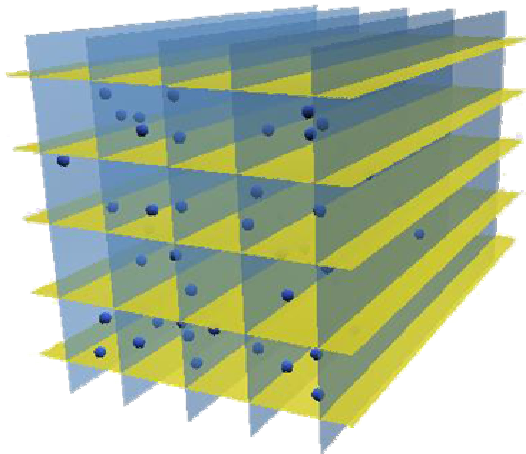


FIG. 1: (Color online) Periodic array of square cross section tubes.

$$(P_i/\alpha_i a_i) \sin(\alpha_i a_i) + \cos(\alpha_i a_i) = \cos(k_i a_i), \quad (4)$$

with $\alpha_i^2 \equiv 2m\varepsilon_{k_i}/\hbar^2$, where $i = x$ or y . We rewrite the dimensionless constants $P_i = mv_i a_i/\hbar^2$ as $P_i = (mv_i \lambda_0/\hbar^2)(a_i/\lambda_0) \equiv P_{0i}(a_i/\lambda_0)$, where $\lambda_0 \equiv h/\sqrt{2\pi m k_B T_0}$ is the de Broglie thermal wavelength of an ideal boson gas in an infinite box at the critical temperature $T_0 = 2\pi\hbar^2 n_B^{2/3}/mk_B \zeta(3/2)^{2/3} \simeq 3.31\hbar^2 n_B^{2/3}/mk_B$ with $n_B \equiv N/L^3$ the boson number density and a_i the distance between the delta barriers along the $i = x$ and y directions. P_{0i} is a measure of the tube wall impenetrability directly related to the delta-barrier strength. This can be understood if we recall the transmission coefficient for a one dimensional delta potential of strength v_i , $\tau_i = 1/(1 + P_{0i}^2/\bar{E})$,⁴¹ with P_{0i} as defined above and \bar{E} is the energy, in $\hbar^2/2ma^2$ units, of particles arriving at right angles with the delta potential. We recover the following two limits: when P_{0i} goes to infinity the transmission coefficient vanishes and our model becomes an infinite number of decoupled tubes; when $P_{0i} = 0$, $\tau_i = 1$ and the confining tube walls disappear recovering the 3D ideal Bose gas. By performing a series expansion of the left-hand-side of (4) just above of the exact P_i -dependent single-particle-ground-state energy ε_{0i} in the first band, the single-particle energy spectrum can be written to first order as

$$\varepsilon_{k_i} \simeq \varepsilon_{0i} + \frac{\hbar^2}{M_i a_i^2} (1 - \cos k_i a). \quad (5)$$

This is the dispersion that has been considered by several authors^{42,43} in the standard nearest-neighbor hopping approximation of the well-known Hubbard model with $\varepsilon_{0i} = 0$. The effective mass M_i is given by the expression

$m[(\alpha_{0i} a_i)^{-1} \sin \alpha_{0i} a_i + P_i (\sin \alpha_{0i} a_i - \cos \alpha_{0i} a_i) (\alpha_{0i} a_i)^{-3}]$ with $\alpha_{0i} a_i = \sqrt{2m\varepsilon_{0i}/\hbar^2}$ and valid for $P_i \gtrsim 0.06$. As expected, M_i grows when P_i increases and for $P_i \gtrsim 40$ the relation is almost linear. Even though (5) might seem to be a good approximation to calculate the thermodynamic properties of the system⁴³ in the low temperature regime, there are distinct effects, particularly in the specific heat, that can only be observed when the full band spectrum is considered as is shown below.

III. CRITICAL TEMPERATURE AND SPECIFIC HEAT

A. Grand potential

The thermodynamic properties of the system are obtained from the grand potential $\Omega(T, L^3, \mu)$ for a boson gas

$$\begin{aligned} \Omega(T, L^3, \mu) &= U - TS - \mu N \\ &= \Omega_0 + k_B T \sum_{\mathbf{k} \neq 0} \ln[1 - e^{-\beta(\varepsilon_{\mathbf{k}_i} - \mu)}] \end{aligned} \quad (6)$$

where Ω_0 is the contribution of the ground state $k_i = 0$ with $i = x, y, z$, and $\beta \equiv 1/k_B T$. As usual, U , S and μ denote the internal energy, the entropy and the chemical potential respectively. By using the dispersion relations given by (3) and (4) and after some algebra we obtain

$$\begin{aligned} \Omega(T, L^3, \mu) &= k_B T \ln[1 - e^{-\beta(\varepsilon_0 - \mu)}] - \frac{L^3 m^{1/2}}{(2\pi)^{5/2} \hbar \beta^{3/2}} \times \\ &\int_{-\infty}^{\infty} \int_{-\infty}^{\infty} dk_x dk_y g_{3/2}(e^{-\beta(\varepsilon_{k_x} + \varepsilon_{k_y} - \mu)}), \end{aligned} \quad (7)$$

where we have replaced the summations by integrals $\sum_{\mathbf{k}} \rightarrow (L/2\pi)^3 \int d^3\mathbf{k}$, assuming $\hbar^2/mL^2 \ll k_B T$, and we have introduced the Bose functions⁴⁴ $g_\sigma(t) \equiv \sum_{l=1}^{\infty} t^l/l^\sigma$. $\varepsilon_0 = \varepsilon_{0x} + \varepsilon_{0y}$ is the ground state energy which depends on P_{0i} and on a_i/λ_0 .

From (7) the thermodynamic properties for a monoatomic gas can be calculated using the relations

$$\begin{aligned} N &= - \left(\frac{\partial \Omega}{\partial \mu} \right)_{T, L^3}, \quad U(T, L^3) = -k_B T^2 \left[\frac{\partial}{\partial T} \left(\frac{\Omega}{k_B T} \right) \right]_{L^3, \mu} \\ \text{and } C_V &= \left[\frac{\partial}{\partial T} U(T, L^3) \right]_{N, L^3}. \end{aligned} \quad (8)$$

where $z \equiv \exp(\beta\mu)$ is the fugacity.

B. Critical temperature

We define the critical temperature T_c as the temperature when the number of bosons in the ground-state level ceases to be negligible, i.e., $N_0(T_c) \simeq 0$ and the chemical potential $\mu(T_c) \simeq \mu_0 = \mu_{0x} + \mu_{0y} = \varepsilon_0$.

From the first expression in Eq. (8) and Eq. (7) we obtain the particle number N

$$N = \frac{1}{e^{\beta(\varepsilon_0 - \mu)} - 1} + L^3 \sqrt{\frac{m}{2\pi^5 \hbar^2 \beta}} \times \int_0^\infty \int_0^\infty dk_x dk_y g_{1/2}(e^{-\beta(\varepsilon_{k_x} + \varepsilon_{k_y} - \mu)}). \quad (9)$$

At $T = T_c$, the first term vanishes and the critical temperature is obtained from

$$\frac{N}{L^3} = \sqrt{\frac{m}{2\pi^5 \hbar^2 \beta_c}} \int_0^\infty \int_0^\infty dk_x dk_y \times g_{1/2}(e^{-\beta_c(\varepsilon_{k_x} + \varepsilon_{k_y} - \mu_0)}). \quad (10)$$

Here we set the number density N/L^3 equal to that of an ideal Bose gas (IBG) in the thermodynamic limit, with a BEC critical temperature T_0 . Note that all the integrals involving the energy-spectrum in the x and y directions can be split in a sum of integrals over the energy bands folded in the first Brillouin zone.

In the *isotropic* case, where $P_{0x} = P_{0y} \equiv P_0$ and $a_x = a_y \equiv a$, the critical temperature as a function of the parameter P_0 is shown in Fig. 2 for different values of the tube cross-section. Note that as the impermeability P_0 of the tube walls increases, the critical temperature diminishes monotonically from T_0 . In contrast, the variation of T_c as function of a/λ_0 shows a non-monotonic behavior (Fig. 3), decreasing for $a/\lambda_0 \lesssim 1$ and increasing otherwise .

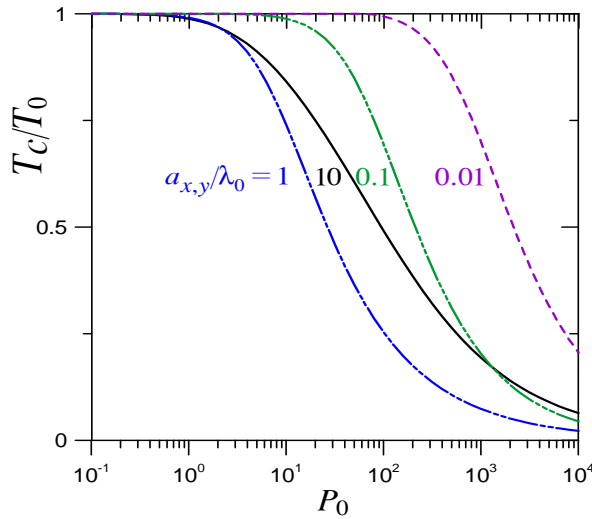


FIG. 2: (Color online) Critical temperature in units of T_0 as a function of P_0 for different values of $a_x/\lambda_0 = a_y/\lambda_0 = a/\lambda_0$.

For both Figs. 2 and 3, we find a similar qualitative behavior of the critical temperature as that reported for a boson gas in multilayers^{38,39}, namely a decrease in T_c/T_0 as P_0 increases and a trend of T_c/T_0 to go back to unity as a/λ_0 increases after having reached a minimum. However, we notice that for similar P_0 and a values as those

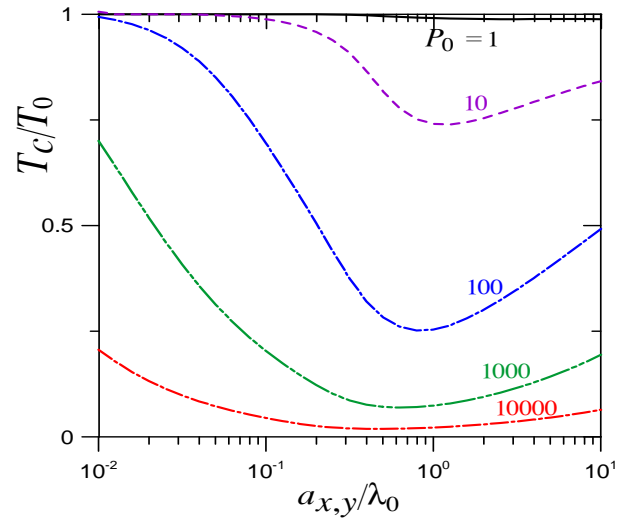


FIG. 3: (Color online) Critical temperature in units of T_0 as a function of $a_x/\lambda_0 = a_y/\lambda_0 = a/\lambda_0$, for different values of P_0 .

used in multilayers, we obtain even lower T_c/T_0 values for bosons in square cross-section tube bundles, showing that the presence of an additional KP delta potential in the two-dimensional array emphasizes even more the effects of confinement. Although we have only shown the critical temperatures for the isotropic case, we will show in the following sections, the effects of anisotropy in the internal energy and specific heat by considering a rectangular cross-section.

C. Internal Energy

The temperature-dependent internal energy U is given by

$$U - \varepsilon_0 N = L^3 \sqrt{\frac{m}{2\pi^5 \hbar^2 \beta}} \int_0^\infty \int_0^\infty dk_x dk_y \times \left\{ (\varepsilon - \varepsilon_0) g_{1/2}(\chi) + \frac{1}{2\beta} g_{3/2}(\chi) \right\}, \quad (11)$$

where $\varepsilon \equiv \varepsilon_{k_x} + \varepsilon_{k_y}$ and $\chi \equiv e^{-\beta(\varepsilon - \mu)}$.

In Fig. 4 we show the internal energy referred to the system ground state energy, for a square cross section, $a_x = a_y$, and in Fig. 5 we show results when a_x is different from a_y . In the isotropic case, the internal energy curves increase monotonically for $a_{x,y}$ larger than λ_0 . However, when the separation is $a_{x,y}/\lambda_0 \simeq 0.5$ or lower, the effect of the KP potentials is revealed by two maxima that become more pronounced as the tube cross-section decreases. This behavior of the internal energy is similar, albeit more complex, in the anisotropic case where the maxima and minima of the corresponding isotropic cases are still present. Minima are associated with the loss of freedom of particles in two directions, which we

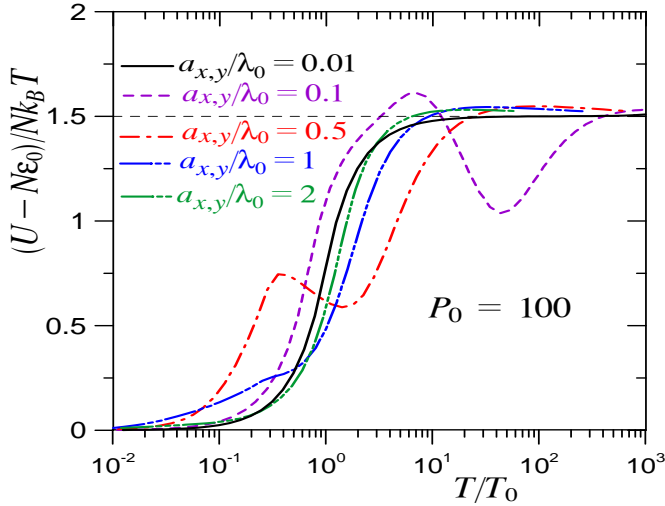


FIG. 4: (Color online) Isotropic case. Internal energy as a function of T/T_0 , for tube arrays of square cross section of several side sizes $a_x/\lambda_0 = a_y/\lambda_0$ and $P_0 = 100$.

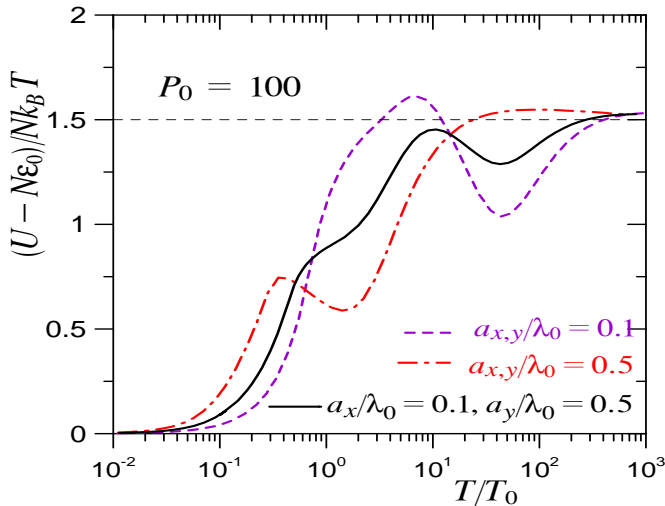


FIG. 5: (Color online) Anisotropic case. Internal energy as a function of T/T_0 , $a_x/\lambda_0 = 0.5$, $a_y/\lambda_0 = 0.1$ and $P_0 = 100$ (black line.) For comparison, the isotropic curves are also shown (color lines).

will discuss in more detail when we analyze the specific heat behavior.

D. Specific heat

From Eq. (8) and (11), the specific heat becomes

$$\frac{C_V}{Nk_B} = \frac{L^3}{N} \sqrt{\frac{m\beta}{8\pi^5 \hbar^2}} \int_0^\infty \int_0^\infty dk_x dk_y \left[g_{1/2}(\chi) \times (2\varepsilon - \varepsilon_0 - \mu + T \frac{d\mu}{dT}) + 2\beta(\varepsilon - \varepsilon_0)g_{-1/2}(\chi)(\varepsilon - \mu + T \frac{d\mu}{dT}) + \frac{3}{2\beta}g_{3/2}(\chi) \right] \quad (12)$$

For $T < T_c$ the chemical potential $\mu = \mu_0$ is a constant, $\partial\mu/\partial T = 0$ and, using $\chi_0 \equiv e^{-\beta(\varepsilon - \mu_0)}$ the last equation for the specific heat becomes

$$\frac{C_V}{Nk_B} = \frac{L^3}{N} \sqrt{\frac{m\beta}{2\pi^5 \hbar^2}} \int_0^\infty \int_0^\infty dk_x dk_y \left\{ g_{1/2}(\chi_0)(\varepsilon - \mu_0) + \beta(\varepsilon - \mu_0)g_{-1/2}(\chi_0)(\varepsilon - \mu_0) + \frac{3}{4\beta}g_{3/2}(\chi_0) \right\}. \quad (13)$$

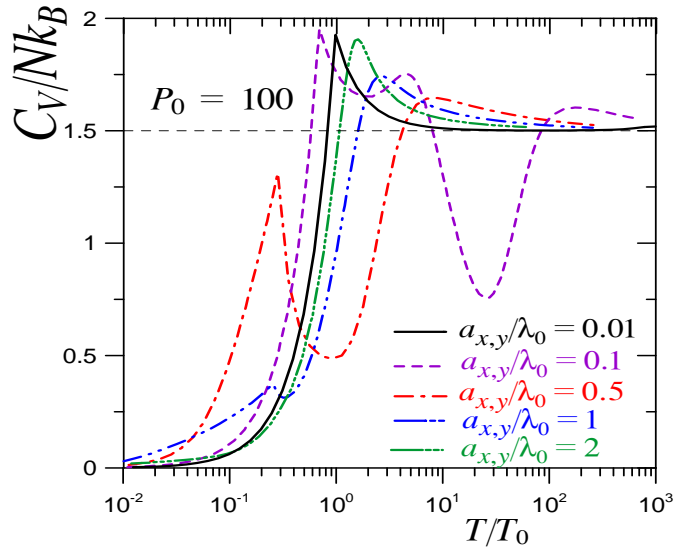


FIG. 6: (Color online) Isotropic case. Specific heat in Nk_B units, as a function of T/T_0 , for different $a_x = a_y$ values and $P_0 = 100$.

In Fig. 6 we show the specific heat for the isotropic case, as a function of T/T_0 for different values of $a_x = a_y = a$ and P_0 fixed to 100. The BEC critical temperature of the system is displayed as a sharp peak in the specific heat that occurs at temperature whose value is lower than the critical temperature of a free ideal Bose gas. Except for the case with $a_x/\lambda_0 = 0.1$ where two minima appear, the specific heat shows only one minimum at a characteristic temperature that reveals the only length scale of the system, namely $a_x = a_y$. Such temperature satisfies the relation $\lambda \simeq 2a_x$ and marks the maximum effects of confinement, where $\lambda = (2\pi\hbar^2/mk_B T)^{1/2}$ is the

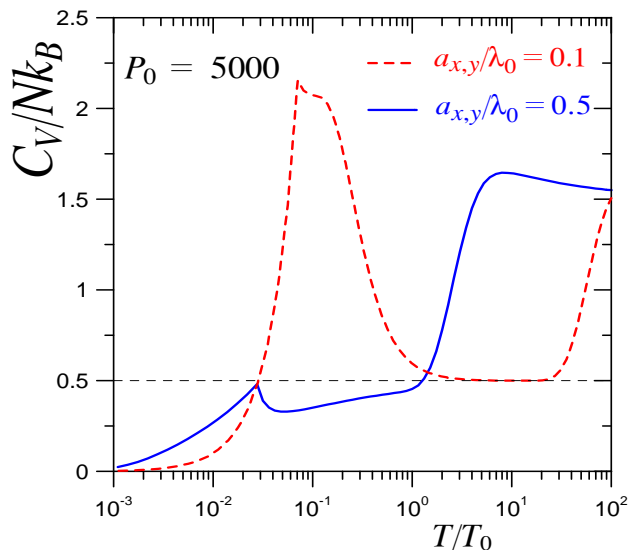


FIG. 7: (Color online) Specific heat in Nk_B units, as a function of T/T_0 , for $P_0 = 5000$, $a_x/\lambda_0 = a_y/\lambda_0 = 0.5$ and 0.1

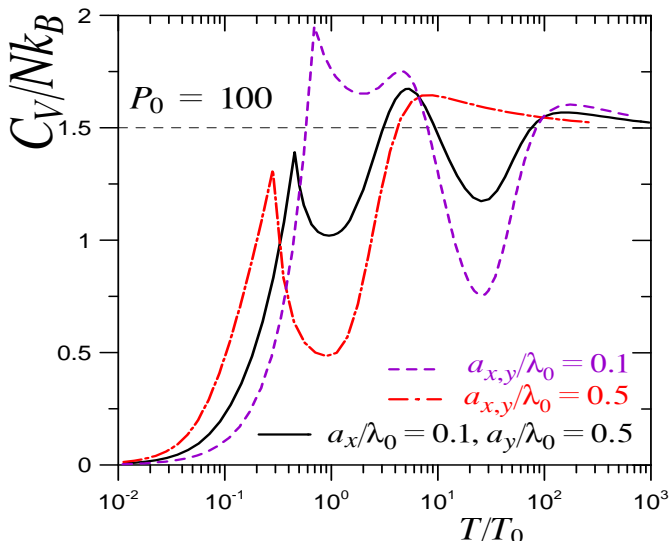


FIG. 8: (Color online) Anisotropic case. Specific heat in Nk_B units, as a function of T/T_0 , for $a_x/\lambda_0 = 0.5$ and $a_y/\lambda_0 = 0.1$ and $P_0 = 100$ (black line) compared to their respective isotropic cases: $a_x/\lambda_0 = a_y/\lambda_0 = 0.1$ and 0.5 , (color lines).

boson thermal-wavelength. There is another characteristic temperature for which the boson thermal wavelength is less than or equal to approx. $0.7 a_x$ that marks the point at which the effects of the walls are less conspicuous, above this temperature the system shows the usual 3D free IBG behavior. The onset of this 3D behavior is observed as the last maximum on the right in the specific heat curve.

As P_0 becomes larger, the specific heat of the isotropic case reveals a *one-dimensional* behavior in a particular range of temperatures determined by the length scale

a , as is shown in Fig. 7. In both cases, $a_x/\lambda_0 = a_y/\lambda_0 = 0.5$, and 0.1 the specific heat C_V/Nk_B , approaches the one-dimensional classical value $1/2$ over a relatively large region of temperatures. This behavior is more pronounced as P_0 is increased.

In Fig. 8 we can see that for the *anisotropic* case where $a_x \neq a_y$, the BEC transition occurs at a temperature between the respective critical temperatures for the isotropic cases $a = \max\{a_x, a_y\}$ and $a = \min\{a_x, a_y\}$, and that the minimum corresponding to each isotropic case, both appear in the anisotropic one.

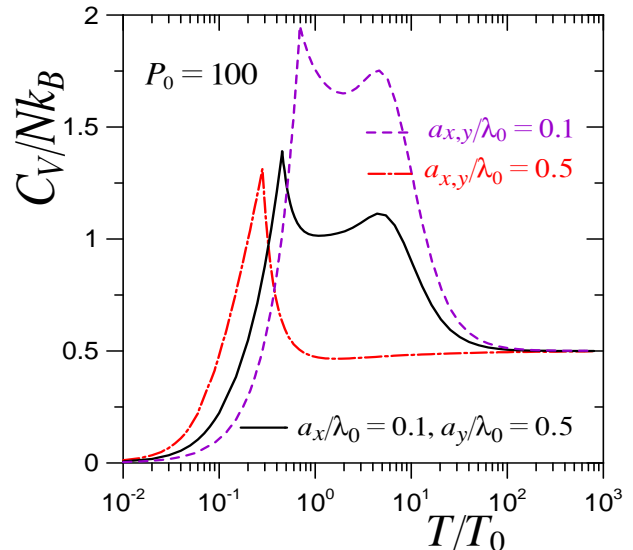


FIG. 9: (Color online) Specific heat in Nk_B units, as a function of T/T_0 , for $a_x/\lambda_0 = 0.5$ and $a_y/\lambda_0 = 0.1$ and $P_0 = 100$ (black line) compared to their respective isotropic cases: $a_x/\lambda_0 = a_y/\lambda_0 = 0.1$ and 0.5 , (color lines). One band only.

E. Density of states

The effects of the band structure are conspicuously exhibited in the density of states (DOS)

$$g(\epsilon) = \sum_{k_x, k_y, k_z} \delta(\epsilon - \epsilon_{k_x} - \epsilon_{k_y} - \epsilon_{k_z}), \quad (14)$$

which can be written in the thermodynamic limit as

$$g(\epsilon) = \frac{L^3}{(2\pi)^3} \sum_{j_x, j_y=1}^{\infty} \int_{-\pi/a_x}^{\pi/a_x} dk_x \int_{-\pi/a_y}^{\pi/a_y} dk_y \int_{-\infty}^{\infty} dk_z \delta(\epsilon - \epsilon_{k_x, j_x} - \epsilon_{k_y, j_y} - \epsilon_{k_z}), \quad (15)$$

where we have explicitly written the integrals over the energy-spectrum in the x and y directions as a sum over bands of the integrals over k_x and k_y in the first Brillouin zone.

Upon integration over dk_z we obtain

$$g(\epsilon) = \frac{L^3}{(2\pi)^3} \left(\frac{2m}{\hbar^2} \right)^{1/2} \sum_{j_x, j_y=1}^{\infty} \int_{-\pi/a_x}^{\pi/a_x} dk_x \int_{-\pi/a_y}^{\pi/a_y} dk_y \frac{\theta(\epsilon - \epsilon_{k_x j_x} - \epsilon_{k_y j_y})}{\sqrt{(\epsilon - \epsilon_{k_x, j_x} - \epsilon_{k_y, j_y})}}, \quad (16)$$

where $\theta(x)$ is the Heaviside step function. For energies close to the minimum, $g(\epsilon)$ varies as $\epsilon^{1/2}$ as it does the DOS of a free particle in three dimensions. This can be shown by noting that for energies close to ϵ_{0i} and for small k , expression (5) can be approximated by $\epsilon_{i0} + \hbar^2 k_i^2 / 2M_i$. In the isotropic case ($\epsilon_{x0} = \epsilon_{y0} = \epsilon_0/2$ and $M_x = M_y = M$), we can therefore write

$$g(\tilde{\epsilon}) \simeq \frac{L^3}{(2\pi)^3} \left(\frac{2m}{\hbar^2} \right)^{1/2} 2\pi \int_0^{\tilde{k}} dk k \frac{\theta(\tilde{\epsilon} - \frac{\hbar^2}{2M} k^2)}{\sqrt{\tilde{\epsilon} - \frac{\hbar^2}{2M} k^2}},$$

where $\tilde{\epsilon} \equiv \epsilon - \epsilon_0$, $k^2 = k_x^2 + k_y^2$ and \tilde{k} is the maximum value of k in the first Brillouin zone. The exact value is not needed as long as $\tilde{\epsilon} < (\hbar^2/2Ma^2) \tilde{k}^2$. Thus, after evaluating the integral by a change of variable we obtain

$$g(\tilde{\epsilon}) \simeq \frac{L^3}{(2\pi)^2} \left(\frac{2m}{\hbar^2} \right)^{1/2} \frac{2M}{\hbar^2} \tilde{\epsilon}^{1/2}. \quad (17)$$

The DOS $g(\epsilon)$ from Eq. (16) is plotted in Fig. 10 for

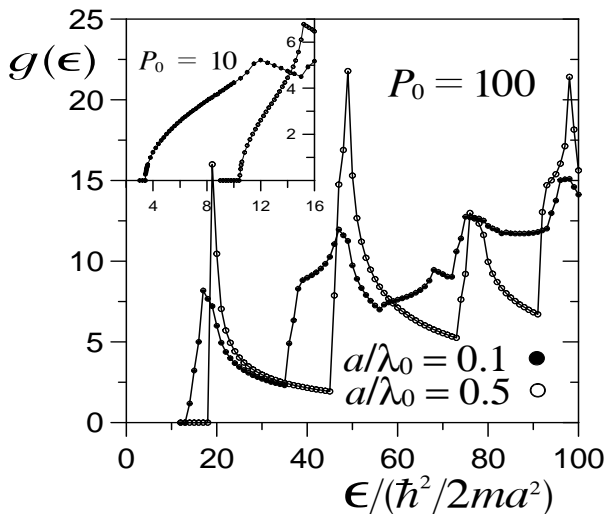


FIG. 10: Density of states for tubes with $P_0 = 100$, $a/\lambda_0 = 0.1$ (full dots) and $a/\lambda_0 = 0.5$ (open dots).

$P_0 = 100$, $a_x/\lambda_0 = a_y/\lambda_0 = 0.1$ and 0.5 . For energies around the bottom of the first band given by (17) is shown in the inset where a smaller value of P_0 has been used to reveal the 3D behavior. The P_0 dependence of $g(\epsilon)$ enters only through the effective mass M , and in general, $g(\epsilon)$ is a rather complex function of the energy (full-dotted curve), however, in the limit of large values of

P_0 the reminiscent behavior $\epsilon^{-1/2}$ of the one-dimensional DOS of a free particle is observed as a “falling” (see for instance the curve in open-circles) of $g(\epsilon)$ with ϵ . This behavior occurs when the energy-states along the z direction are the only ones that contribute to $g(\epsilon)$, the contribution due to the other two directions being a constant related to the energy band-gaps.

IV. DISCUSSION AND CONCLUSIONS

At this point let us make the following remarks. In Fig. 9 we plot C_V as a function of T/T_0 for different plane separations and $P_0 = 100$, where *only* the first energy band, exactly computed from Eq. (4) in the x - and y -directions, has been considered. This situation qualitatively resembles the results obtained if the dispersion relation (5) were used^{42,43}. We consider the corresponding calculation of C_V in Fig. 8, where we have used enough number of exact energy bands needed to achieve the required precision in the calculation of this property. We note that both curves coincide quantitatively and qualitatively for temperatures not greater than T_0 ; for temperatures between T_0 and about $5 T_0$ the qualitatively behavior remains best for the smaller plane separations; finally, for temperatures greater than $5 T_0$ even the qualitative agreement disappears. Important structural information is missing when just one band is included in the calculation, for instance, the second minimum that appears in the isotropic case of Fig. 8 (full-black line) is missing in the corresponding curve in Fig. 9. Clearly, the use of the lowest band leads to a one-dimensional behavior in the classical limit even though the system is three-dimensional.

In the isotropic case (that can be related to homogeneous nanotubes bundle-system), our model predicts a one-dimensional behavior of the specific heat in a range of temperatures determined by the distance between the delta-barriers. Such results shown in Fig. 7 can be used to comparatively explain the one dimensional character of the specific heat of adsorbed ^4He in single-wall nanotubes as expected and observed in experimental situations³⁰. Although Lasjaunias et al. did not report the presence of the peak that marks the BEC phase-transition we explain this fact in terms of the finite size of the experimental system where such transition can be made much less conspicuous.

One important result is that our system always exhibits a BEC which is possible due to the coupling between the different channels the bosons move in. When the wall impenetrability goes to infinity our system becomes a set of decoupled tubes with zero BEC critical temperature as expected. Some results, often found in the literature, which claim that BEC in a bundle of homogeneous nanotubes is not possible³¹, agree with ours if homogeneous means non-communication among tubes. However in the experimental set up, it is clear that the heterogeneity of the interstitial channels may have strong

effects on the thermodynamic behavior of the system, in particular in the BEC critical temperature which can be different from zero if the heterogeneity of the channels causes exchange of atoms among them.

On the other hand, the use of multifilamentary superconducting tapes⁴⁵ or wires³³ has improved the coil performance to support higher critical current density useful to create higher magnetic field to be used, for example, in the Large Hadron Collider currently under operation or the International Thermonuclear Experimental Fusion Reactor planned to work in 2019. In both cases tapes and wires gather many filaments where pairs flow preferentially along the longitudinal direction. Critical temperature distribution in the Nb₃Sn strands as well as the specific heat have been reported. The authors point out two transitions in the specific heat curve: one at the critical temperature (around 18 K) they associate to the complex superconductor wire and another one at a lower temperature (around 9 K) they associate to the unreacted Nb. However, if the Cooper pairs should be considered as bosons, our specific heat calculations show at least two critical temperatures: the lower one associated to the collective effect of the filaments (our tubes) and a smooth maximum corresponding to the boson gas behavior in the individual filaments. In other words, the meaning given to the maxima in our Fig. 8 and in the Fig. 4 of Ref. [33], are interchanged. A way to elucidate this controversy would be to make wires with larger filament diameters, then prove that their smooth maximum shifts to the left as it is observed in our calculations.

We summarize our main results in the following list: we observe that in the presence of periodical structures constructed with orthogonal Dirac combs inside an infinite box filled with bosons, the critical temperature decreases from the 3D ideal boson gas T_0 as P_0 increases, while the plane separations $a_{x,y}/\lambda_0$ are kept constant. It becomes zero when the periodic delta potential strengths become infinite. In other words, there is not BEC critical tem-

perature different from zero for bosons in a tube of finite cross section and infinite length.

As the separation between planes is lowered, the critical temperature reaches a P_0 -dependent minimum value and then it is expected^{38,39} to increase again towards T_0 .

For systems with $a_{x,y} > \lambda_0$ the numerical calculations for the critical temperature and specific heat are very sensitive to the number of energy bands considered. To attain convergence we need to include up to 1000 bands.

At $T = T_c$, the specific heat is continuous but has a discontinuity in its derivative. In the isotropic case it has one minimum and one or two maxima. The minimum is associated to particle trapping between two planes when its thermal wavelength is equal to $2a$. This is corroborated in the anisotropic case where the specific heat shows not one but *two* minima associated with the particle trapping in the x or y directions.

The maximum at higher temperatures is associated to the onset of the system's approach to a 3D IBG behavior in this regime where the thermal wavelength $\lambda \lesssim 0.7a$.

While there is still a controversy over whether or not Bose-Einstein condensation of ⁴He exists inside interstitial filaments in bundles of carbon nanotubes, we conclude that in order to have BEC there must be a way through which the interstitial channels are coupled among them, either by effects of inhomogeneity of the tube bundles or by tunneling across the weaker interstitial walls.

Finally, we mention that the proposed model in this paper gives account of systems composed of a very large number of quasi-one dimensional systems such as: bundles of carbon nanotubes, superconductor-multistrand wires, Bechgaard salt or 2D opto-magnetic traps.

We acknowledge the partial support from grant PA-PIIT IN105011, IN117010-3, and IN106908. CONACyT 104917.

-
- ¹ N.D. Mermin and H Wagner, Phys. Rev. Lett. **17**, 1133 (1966).
² P.C. Hohenberg, Phys. Rev. **158**, 383 (1967).
³ J.M. Kosterlitz and D.J. Thouless, J. Phys. C: Solid State Phys. **6**, 1181 (1973).
⁴ J.M. Kosterlitz, J. Phys. C: Solid State Phys. **7**, 1046 (1974).
⁵ A.F. Hebard, Phys. Rev. Lett. **44**, 291 (1980).
⁶ L Benfatto, C Castellani, T Giamarchi, Phys. Rev. Lett. **98**, 117008 (2007).
⁷ B I Halperin, D R Nelson, J. Low Temp. Phys. **36**, 599 (1979).
⁸ L.A. Turkevich, J. Phys. C: Solid State Phys. **12**, L385 (1979).
⁹ S Doniach, BA Huberman, Phys. Rev. Lett. **42**, 1169 (1979).
¹⁰ T. Ota, I. Tsukada, I. Terasaki, K. Uchinokura arXiv:cond-mat/9405027v2.
¹¹ D. J. Bishop, J. D. Reppy, Phys. Rev. Lett. **40**, 1727 (1978).
¹² G. Agnolet, D. F. McQueeney, J. D. Reppy, Phys. Rev. B **39**, 8934 (1989).
¹³ D. R. Luhman, R. B. Hallock, Phys. Rev. Lett. **93**, 086106 (2004).
¹⁴ H.J. Lauter, H. Godfrin, V. L. P. Frank, and P. Leiderer, Phys. Rev. Lett. **68**, 2484 (1992).
¹⁵ L. M. Steele, C. J. Yeager, and D. Finotello, Phys. Rev. Lett. **71**, 3673 (1993).
¹⁶ K. Shirahama, K. Yamamoto and Y. Shibayama, J. Phys. Soc. Jpn. **77**, 111011 (2008).
¹⁷ K. Yamamoto, Y. Shibayama and K. Shirahama, Phys. Rev. Lett. **100**, 195301 (2008).
¹⁸ J.G. Dash and J. Ruvalds, *Phase Transitions in Surface Films*, NATO Advanced Study Institutes Series B Vol. 51 (Plenum, NY, 1980).
¹⁹ L.W. Brunch, M.W. Cole and E. Zaremba, *Physical Ad-*

- sorption: Forces and Phenomena* (Oxford University Press, Oxford, 1997).
- ²⁰ E. H. Lieb and D. C. Mattis, *Mathematical Physics in One Dimension* (Academic Press, NY, 1966).
 - ²¹ S. Burger, K. Bongs, S. Dettmer, W. Ertmer, and K. Sengstock, Phys. Rev. Lett. **83**, 5198 (1999).
 - ²² M. Greiner, I. Bloch, O. Mandel, T. W. Hänsch, and T. Esslinger, Phys. Rev. Lett. **87**, 160405 (2001).
 - ²³ S. R. Clark and D. Jaksch, Phys. Rev. A **70**, 043612 (2004).
 - ²⁴ S. Iijima, Nature (London) **354**, 56 (1991).
 - ²⁵ A. Thess, R. Lee, P. Nikolaev, H. Dai, P. Petit, J. Robert, C. Xu, Y. H. Lee, S. G. Kim, A. G. Rinzler, D. T. Colbert, G. E. Scuseria, D. Tomanek, J. E. Fischer, R. E. Smalley, Science **273**, 483 (1996).
 - ²⁶ W. Teizer and R. B. Hallock, Phys. Rev. Lett. **82**, 5305 (1999).
 - ²⁷ Z. Wang, J. Wei, P. Morse, J.G. Dash, O.E. Vilches, D.H. Cobden, Science **327**, 552 (2010).
 - ²⁸ F. Ancilotto, M. M. Calbi, S. M. Gatica, and M. W. Cole, Phys. Rev. B **70**, 165422 (2004).
 - ²⁹ B. Marcone, E. Orlandini, F. Toigo, and F. Ancilotto, Phys. Rev. B **74**, 085415 (2006).
 - ³⁰ J.C. Lasjaunias, K. Biljaković, J.L. Sauvajol and P. Monceau, Phys. Rev. Lett. **91**, 025901 (2003).
 - ³¹ S.M. Gatica, M.M. Calbi, R.D. Diehl and M.W. Cole, J. Low Temp. Phys. **152**, 89 (2008).
 - ³² W. Shi and J. K. Johnson, Phys. Rev. Lett. **91**, 015504 (2003).
 - ³³ C. Senatore, D. Uglietti, V. Abacherli, A. Junod and R. Flukiger, IEEE Trans. on App. Supercond. **17**, 2611 (2007).
 - ³⁴ T. Miyazaki, T. Hase and T. Miyatake, in *Handbook of Superconductor Materials*, D. A. Cardwell and D. S. Ginley eds. (Institute of Physics Publishing, Bristol and Philadelphia, 2003) p639.
 - ³⁵ Y. Wang, C. Senatore, V. Abacherli, D. Uglietti and R. Flukiger, Supercond. Sci. Technol. **19**, 263 (2006).
 - ³⁶ B. Seeber, C. Senatore, F. Buta, R. Flukiger, T. Boutboul, C. Scheuerlein, L. Oberli and L. Rossi, WAMSDO Proceedings, p37 (2008).
 - ³⁷ F. Pesty, P. Garoche and K. Bechgaard, Phys. Rev. Lett. **55** (1985) 2495.
 - ³⁸ P. Salas, M. Fortes, M. de Llano, F.J. Sevilla and M.A. Solís, J. Low Temp. Phys. **159**, 540 (2010).
 - ³⁹ P. Salas, F.J. Sevilla, M. Fortes, M. de Llano, A. Camacho and M.A. Solís, Phys. Rev. A **82**, 033632 (2010).
 - ⁴⁰ Kronig R. de L. and Penney W.G., Proc. Roy. Soc. (London), A **130**, 499 (1930); McQuarrie, D. A. *The Kronig-Penney Model: A Single Lecture Illustrating the Band Structure of Solids*, The Chemical Educator **1**, 1 (Springer-Verlag New York, INC. (1996).
 - ⁴¹ M. de Llano, *Mecánica Cuántica* 2a. Ed. (Las prensas de ciencias, Fac. de Ciencias, UNAM, 2002) p. 51; D. J. Griffiths, *Introduction to Quantum Mechanics* (Prentice Hall, New Jersey, 1995) p. 57.
 - ⁴² X.-G. Wen and R. Kan, Phys. Rev. B **37**, 595 (1988).
 - ⁴³ A. Hærdig and F. Ravendal, Eur. J. Phys. **14**, 171 (1993).
 - ⁴⁴ R.K. Pathria, *Statistical Mechanics*, 2nd Ed. (Pergamon, Oxford, 1996).
 - ⁴⁵ F. Sumiyoshi, A. Kawagoe, T. Furubeppu and Y. Hoshira, J. Phys.: Conf. Series **234**, 022038 (2010).